CLM-P 306

CLM-P 306

UKAEA RESEARCH GROUP

Preprint

INSTABILITY, FUSION AND FISSION OF ASYMMETRIC VORTEX STRUCTURES

J P CHRISTIANSEN
N J ZABUSKY

CULHAM LABORATORY
Abingdon Berkshire

1972

CLM-P 306

INSTABILITY, FUSION AND FISSION OF ASYMMETRIC VORTEX STRUCTURES

by

J P Christiansen and N J Zabusky*

(Submitted for publication in Journal of Fluid Mechanics)

ABSTRACT

We have made computational experiments to study the stability and long-time evolution of two-dimensional wakes. We have used the VORTEX code, a finite-difference realization of two-dimensional incompressible inviscid fluids. In the first experiment an initial shear-unstable triangular velocity profile evolves into a non-homogeneous finite-area, asymmetric vortex array and like-signed regions attract and fuse (or coalesce). Enhanced transport across the profile is due to "capture" and convection of small-scale vortex regions by larger oppositely signed vortex regions. In the following experiments we study the stability of an asymmetric four-vortex finite-area system corresponding to a von Kármán street of point vortices. Here the critical parameter is b/a, the initial transverse-to-longitudinal separation of vortex centers. At b/a = 0.281 the four-vortex system is stable and we observe large-area vortex regions develop elliptical (m=2), triangular (m=3), etc. surface modes due to self-consistent interactions. At (b/a) = 0 the measured growth rate is smaller than the corresponding von Kármán system and at (b/a) = 0.6 the measured growth rate is larger. At (b/a) = 0 one vortex undergoes fission in the high-shear field produced by two nearest-neighbour oppositely signed vortex regions. Heuristic comparisons are made with the two-dimensional tunnel experiments of Taneda and others.

* Permanent address: Computational Physics Research Department, Bell Laboratories, Whippany, NJ 07981. USA.

UKAEA Research Group
Culham Laboratory
ABINGDON, Berks.

August 1972

1. INTRODUCTION

In recent years there have been renewed efforts to understand the non-linear dynamics of interacting vortex structures in high Reynolds number (high-R) two-dimensional jets and wakes. Carefully controlled experiments (Taneda, 1959 and 1965 and Durgin and Carlson 1970) that minimize three-dimensional effects in low noise wind tunnels have shown that asymmetric vortex structures have a finite life time, i.e.they become unstable . At variable distances downstream (many wavelengths of the fundamental vortex structure), the observed pattern abruptly loses its coherence and degenerates or "breaks down into a less ordered pattern". From this visually chaotic state evolves a secondary asymmetric vortex structure, more diffuse than the primary structure and of longer wavelength. This hierarchy of two-dimensional vortex structures is sufficiently uncomplicated that a deterministic, non-statistical approach should elucidate the basic mechanisms involved. As exemplified below, numerical simulations with a two-dimensional zero-viscosity model can provide such insights.

In flat-plate wake experiments, Sato and Kuriki (1961) also measured the properties of high-R wakes at moderate distances behind flat plates. Their high-quality hot-wire data was interpreted by Zabusky and Deem (1971) in a computational/experimental study as consistent with the motion of an asymmetric wake of elliptical nutating vortices. Zdravkovich (1968 and 1969) and Durgin and Karlson (1970) also found elliptical and other distorted vortex structures to be a common occurrence in wakes of cylinders. The elliptical shape of the vortex is a non-viscous effect due to the mutual interaction of nearby vortex regions.

To clarify the qualitative features of ideal high-R laminar flows downstream of flat plates, it is convenient to describe

phenomena in contiguous spatial regions:

(1) At very short distances one finds nearly laminar flows with a Gaussian type velocity profile. For $R > 10^4$ the inviscid Rayleigh equation provides eigenfunctions and unstable eigenvalues. R is based on the length of the plate. The Reynolds number based on the boundary layer thickness (or radius of a cylinder) is > 500.

(2) At short distances, induced perturbations (via acoustically driven loudspeakers, vibrating ribbons etc.) grow in accordance with linear stability theory. For $R > 10^4$ Sato and Kuriki (1961) and Zabusky and Deem (1971) showed that the Rayleigh equation provides unstable eigenvalues that agree with observations.

(3) At moderate distances the fastest growing modes have the most energy and saturate when a regular asymmetric street of elliptical vortices form. The finite-sized elliptical vortices undergo a slow pitching or nutating motion in the laboratory frame of reference. This phenomenon was also observed in the wake of cylinders and in two-dimensional jets by Beavers and Wilson (1970).

(4) At large distances, the vortex structure may break down, (collapse or undergo a transition) to another asymmetric street, where the longitudinal distance between nearby vortices in the same row can increase by a factor of 2 to 10 depending on the Reynolds number (Taneda, 1959).

(5) At very large distances the break down and reformation of the vortex structure may be repeated several times. However, at very high-R the turbulent or chaotic structure may persist.

In wakes beyond cylinders and other bluff bodies, regions (1) and (2) are inseparable and pockets of vorticity aggregate alternatively on either side. When the vortex concentrations are sufficiently large they are convected away to form an asymmetric street. The rate of convection of vortex aggregations determines the Strouhal number.

For real rather than ideal, high-R flows the above regions may not be clearly separated. The flow configuration at moderate to large distances (particularly at very high-R) is very sensitive to the precise operating conditions and excitation mechanisms, that is the predictability of the flow decreases at large distances or long times. The suppression of 3-dimensional disturbances; the rigidity of the mounting; the smoothness of the construction and excitation mechanisms; the quietness of the wind tunnel; and a finite viscosity all contribute to a more predictable result.

Computer simulation studies of the stability of wake-like configurations were undertaken because the literature of analytical non-linear treatments is an empty set. We have linear stability theories for symmetric and asymmetric configurations of point vortices begun by von Kármán and elaborated by Kochin, Kibel and Roze (1964). For two oppositely signed streets of point vortex filaments the symmetric configuration is unconditionally unstable. The asymmetric configuration on the other hand is only stable if the transverse to longitudinal separation $(\frac{b}{a})$ is 0.281. However, as emphasized by Kochin, Kibel and Roze (p.226-234) this is a necessary condition: "A first order perturbation theory shows that the positions of vortices in a street with $(\frac{b}{a}) = 0.281$ will separate by a finite amount". Rosenhead (1930) examined the linear stability of the

$(\frac{b}{a}) = 0.281$ asymmetric street for small-but-finite area circular vortex regions. However this calculation is not applicable to strictly 2-dimensional finite area vortex streets, as described below.

Most past analytical and computational work has concentrated on studying point vortex configurations, that is vortex deformations are excluded from the dynamics. The reasons for excluding deformations of finite area vortices can be summarized by quoting Bassett (p. 42 vol. II 1888): "If more than one vortex exists in a fluid, the effect of any one of the vortices upon the others will be to produce a motion of translation combined with a deformation of their cross sections. The mathematical difficulties of solving this problem when the initial distribution of the vortices and the initial forms of their cross sections are given, are very great; and it seems impossible in the present state of analysis to do more than obtain approximate solutions in certain cases".

Our study generalizes and considers finite-area constant density vortices (Rankine vortices) confined by a contour

$$r^2(\theta) = R_o^2 + \sum_m \alpha_m e^{im\theta} + cc ,$$

where r is measured from the vortex centre. (The variable r^2 is used to simplify the verification of area conservation). For $\alpha/R_o^2 \ll 1$ a translation with no distortion corresponds to an $m = 1$ disturbance and an $m = 2$ disturbance results in an elliptic shape. Generally high-m disturbances can arise through close non-linear interactions as shown by Christiansen and Roberts (1969) and by Christiansen, Taylor and Roberts (1972) for two vortices.

There has also been work on wake-like configurations. Using the VORTEX code, Christiansen (1970) studied the instability of a

trapezoidal longitudinal velocity distribution with widely separated flanks and subject to random perturbations. The final state was four staggered elliptically shaped vortices. Solving a finite-difference representation of the Navier-Stokes equation, Deem, Hardin and Zabusky (1971) initially perturbed a laminar Gaussian profile with a second-harmonic plus small-random perturbation and observed the growth of four elliptically shaped vortices of unequal strength. There follows a period of quasi-stationary evolution of the vortex configuration and finally a rapid coalescence of pairs of like-signed vortex regions. Similar phenomena are described below in the simulations of a triangular velocity profile and the evolution of two pairs of oppositely signed asymmetrically placed vortex regions.

2. TWO-DIMENSIONAL IDEAL FLUIDS AND THE VORTEX CODE

The incompressible, inviscid fluid can be described by the coupled continuity and Euler equations

$$\nabla \cdot \underline{u} = 0 , \tag{1}$$

$$\frac{\partial \underline{u}}{\partial t} + \underline{u} \cdot \nabla \underline{u} = - \frac{1}{\rho} \nabla p . \tag{2}$$

These equations describe experiments where local fluid speeds are smaller than the sound speed and dissipation plays a negligible role in the dynamics. For a two-dimensional ideal fluid the vorticity has one component orthogonal to the plane of motion and one can introduce a stream function ψ .

$$\underline{u} = \nabla \times (\underline{e}_z \psi) , \tag{3}$$

$$\zeta = \underline{e}_z \cdot \nabla \times \underline{u} = - \nabla^2 \psi , \tag{4}$$

where $$\nabla = \underline{e}_x \partial_x + \underline{e}_y \partial_y .$$

Substituting (3) and (4) into (2) yields the familiar Liouville equation (analogous to the one-dimensional Vlasov equation of plasma physics)

$$\zeta_t + \psi_y \zeta_x - \psi_x \zeta_y = 0 , \tag{5}$$

that describes a Hamiltonian system with characteristic velocities

$$\dot{x} = \psi_y \qquad \dot{y} = - \psi_x . \tag{6}$$

Any state of the system is described by the vorticity distribution $\zeta(x,y)$ and can evolve into all other states subject to the constraints imposed by the conservation laws:

Linear momentum: $\underline{P} = \rho \iint \underline{u} \, dxdy$, (7)

Angular momentum: $\underline{L} = \rho \iint \underline{r} \times \underline{u} \, dxdy$, (8)

Kinetic energy $E = \frac{1}{2}\rho \iint |\underline{u}|^2 \, dxdy = \frac{1}{2}\rho \iint \zeta\psi \, dxdy$, (9)

Vorticity areas: $A(\zeta) \, d\zeta$, (10)

where $A(\zeta) \, d\zeta$ is the area between two vorticity contours ζ and $\zeta + d\zeta$. Helmholtz's theorem tells us that these areas are convected with the fluid and hence it is convenient to study systems where the vorticity density, ζ, is constant and takes on the values $+\zeta_o$, 0 and $-\zeta_o$. The area conservation law is simply the conservation of area within the contours surrounding these regions.

The numerical experiments have been carried out with the particle/field (vortex filament - stream function or vorticity) VORTEX code (Christiansen 1970). This algorithm is based on the fact that the motion of vortex filaments is described by the ordinary differential equations (6). The stream function is determined from

the distribution of point vortices by numerically inverting the Poisson equation (4). The advantages and deficiencies of this method were studied by Christiansen (1971) for the simple case of a single circular vortex of constant vorticity ζ_o (Rankine vortex). The numerical experiments presented below have been carried out using 3200 positive or negative point vortices that are moved on a cartesian mesh of dimensions 64x64. In general 9 different types of boundary conditions are available. Appendix 1 describes pertinent details of the code's operation.

Errors are inevitable in solutions produced by finite difference methods. In the VORTEX code no attempt is made to enforce conservation or "semi-conservation" (continuous temporal variables) of mass (local incompressibility of the flow), momentum, energy, enstrophy or area. These quantities are monitored to allow one to assess the quality of the run (see Appendix 1). The local violation of incompressibility is manifest in the figures below as a fine wave-like structure, particularly on the surface of the vortex region. One easily resolves this structure on the large-area vortices, e.g. Figure 6 (t = 8.75), Figure 7 (t = 7.5), Figure 11 (t = 7.0). Note that the fine structure becomes sharper and penetrates deeper into the vortex regions at later times, Figure 5 (t = 8.75). Also long "arms" of vorticity are dispersed, indicating that small-scale phenomena are not adequately represented. These short-wavelength truncation errors do not cause instability and apparently do not contribute greatly to the large-scale motions for the duration of our runs.

3. EPITOME OF NUMERICAL EXPERIMENTS

The numerical experiments summarized in this section and outlined in Table 1 are all related to our abstractions of high-R wakes of flat plates or bluff bodies. These are initial-value problems and in discussing laboratory experiments we assume that the time elapsed in a calculation corresponds to distance downstream. Zabusky and Deem (1971) validated this assumption by comparing numerical solutions of the Navier-Stokes equation with the flat-plate wake experiments of Sato and Kuriki. The calculations start from uniform vorticity distributions located in a box with periodic boundary conditions in x and either fixed or periodic boundary conditions in y. Equations 4 and 5 are normalized such that a vorticity density $\zeta_o = \frac{N}{A}$ (N number of point vortices confined to the area A) will produce a rotational period of $T_o = \frac{4\pi}{\zeta_o}$ units of time. The time step in an integration initially satisfies the Courant-Friedrichs-Lewy condition by a wide margin and is taken as

$$\Delta t = C \frac{\Delta x}{<|\underline{v}|>} = (4 <|\underline{v}|>)^{-1} \quad , \tag{11}$$

where

$$<|\underline{v}|> = \frac{1}{N} \sum_{j=1}^{N} |\underline{V}_j| \quad . \tag{12}$$

In section 5 we discuss the laminar triangular longitudinal velocity profile with random perturbations (experiment I) and show that the linearly unstable profile transforms into an asymmetric (staggered) array of unequal strength vortex regions which coalesce or fuse.

In section 6 we begin the study of the stability of four finite area vortex regions, with periodic boundary conditions in the longitudinal (x) direction. The parameters of the study are:

(i) The area of the vortex regions

(ii) The initial shape of the regions

(iii) The transverse boundary conditions (fixed or periodic)

(iv) The nature of the perturbation to one or more vortex regions (lateral or longitudinal displacement of the centroid of a vortex region, shape or size change, etc).

(v) The transverse - to-longitudinal separation $\frac{b}{a}$ of the vortex centers.

Section 6 studies $\frac{b}{a} = 0.281$ (experiments II to V) known to be "marginally" stable for point vortices. For runs of duration 19 circulation periods, we find stability.

In section 7 we treat the case $\frac{b}{a} = 0.6$ known to be unstable for point vortices and we find instability followed by fusion of like-signed vortices. See experiments VI to IX.

In section 8 the standing wave case $\frac{b}{a} = 0$ is treated and we find instability and a peculiar strong dynamical interaction that finally leads to a rapid fission of one vortex followed by fusion of vortex regions in a longer time scale. See experiment X.

The results are visualized by displaying the location of vortex filaments (particles) at separated times. Dark grey areas represent regions of negative vorticity (clockwise rotation) and light grey areas represent regions of positive vorticity (counterclockwise rotation (see figures 3, 5, 6, 7, 8, 9 and 11). A computer-generated

film has been made that vividly demonstrates many of the phenomena. K V Roberts showed and discussed this film at the European conference on Computational Physics (Geneva, April 1972) as part of his talk on a review of numerical methods in fluid dynamics (Roberts and Christiansen (1972).

Expt. No.	$\frac{b}{a}$	Eccentricity of vortices	π^{-1}(Area) of typical vortex	y-boundaries	Elapsed time T_E	No. of timesteps	ζ_o	T_E/T_o
I	Laminar wake		-	F	10.5	1344	6.25	
II	0.281	0.0	9	F	9.0	576	27.0	19.4
III	0.281	0.0	35	P	9.0	576	7.0	5.0
IV	0.281	0.85	26	F	3.0	192	9.4	2.24
V	0.281	0.85	26	F	3.0	192	9.4	2.24
VI	0.6	0.7	35	F	24.0	768	7.0	13.3
VII	0.6	0.7	35	P	6.0	192	7.0	3.3
VIII	0.6	0.0	35	P	6.0	192	7.0	3.3
IX	0.6	0.0	9	P	9.0	1152	27.0	19.4
X	0.0	0.0	35	P	17.0	576	7.0	9.45

TABLE 1. Experiments presented in this paper.

Column 5: F & P mean fixed or periodic y-boundaries. In column 9, $T_o = 4\pi/\zeta_o$ is the rotation period of the vortex.

4. COMMENTS ON PREVIOUS ANALYTICAL WORK

The original calculation by von Kármán for an asymmetric point vortex system has been repeated by Lamb (Section 15b, p.228) and somewhat generalized by Kochin, Kibel and Roze (Section 5.21). If nearest neighbour vortex filaments on the same line (separated by a) are given the same displacement, $x_m = \alpha e^{im\varphi}$, $y_m = \beta e^{im\varphi}$, the solution of the linearized perturbation equations yields the dispersion relation

$$\lambda = (\Gamma_o/2\pi a^2)(\pm iD \pm \sqrt{A^2-C^2}) \quad , \tag{13}$$

where

$$A = \frac{1}{2}\varphi(2\pi-\varphi) - \pi^2/\cosh^2(\pi b/a) \quad , \tag{14}$$

$$B = iD = i\left\{\frac{\pi\varphi\sinh(\pi-\varphi)b/a}{\cosh(\pi b/a)} + \frac{\pi^2\sinh\varphi b/a}{\cosh^2(\pi b/a)}\right\} \quad , \tag{15}$$

$$C = \frac{\pi^2\cosh(\varphi b/a)}{\cosh^2(\pi b/a)} - \frac{\pi\varphi\cosh(\pi-\varphi)b/a}{\cosh(\pi b/a)} \quad . \tag{16}$$

The condition $\varphi = \pi$ is most unstable as it makes $C = 0$ and

$$A = \frac{1}{2}\pi^2[1-2\cosh^{-2}(\pi b/a)] \tag{17}$$

$$B = iD = i\pi^2[\sinh(\pi b/a)\cosh^{-2}(\pi b/a)] \quad . \tag{18}$$

The condition $A = 0$ is necessary for stability and this yields the well-known condition

$$\cosh(\pi b/a) = 1 \quad \text{or} \quad b/a = 0.281 \quad . \tag{19}$$

The oscillation frequency is

$$\text{Im}\ \lambda = \pm\frac{1}{4}\pi\ \Gamma_o/a^2 = \pm\ 0.5895 \tag{20}$$

where the numerical value corresponds to our case, $a = 32$ and $\Gamma_o = \pi R_o^2\ \zeta_o = 766$ (the number of filaments in each vortex region). The growth rates at two values of b/a are

$$b/a = 0.6 \; ; \qquad \lambda = 0.481 \quad , \tag{21}$$

$$b/a = 0 \; ; \qquad \lambda = \frac{1}{4}\pi\Gamma_o/a^2 = 0.590 \quad . \tag{22}$$

Three additional analytical calculations bear on the results below. Kochin, Kibel and Roze (1964, pp.226-234) applied a higher-order perturbation calculation to the asymmetric point vortex street with $b/a = 0.281$. They have shown that the street is always unstable, i.e. arbitrary small displacements will cause vortices to ".... separate by a finite amount". This is not surprising as the Kármán street is unstable for $b/a \gtrless 0.281$. If odd vortices on the upper street are displaced upward by ϵ a configuration results identical to that obtained by increasing the separation to $0.281 + \epsilon/2$ and then displacing positive vortices upwards by $\epsilon/2$ and negative vortices downward by $\epsilon/2$. Since the latter system is linearly unstable, it would be reasonable to assume that the former system is unstable to finite amplitude disturbances.

Rosenhead (1929, 1930) has extended the von Kármán linear analysis by examining the effects of transverse free-slip boundaries (1929) and the effects of 3-dimensional/small-area regions (1930). In the first study Rosenhead assumed point vortices that if fixed y-boundaries are introduced at a distance $\pm h/2$ from the centre of the street, the b/a ratio for "stability" decreases from 0.281 to 0.256 as a/h increases from 0 to 0.815. As a/h is increased further, the b/a line becomes a region or area of stability. Rosenhead gives a formula for the modified stability line as

$$b/a = 0.281 - 0.090(a/h)^6 = .280 \quad ,$$

where we have used our ratio $a/h = 0.5$. (See Rosenhead, Equation (5), p.321. N.B. Rosenhead uses: 2b for the longitudinal distance between vortices; 2a for the transverse distance between vortices

and 2c for the distance between fixed walls). In comparison with finite area the transverse boundaries play a negligible role.

In the second study (1930), Rosenhead purports to treat finite-area effects but in fact mixes 3-dimensional considerations with small-area 2-dimensional considerations. He states, "The problem in its initial stages can no longer be treated as one in two dimensions for the "self-induction" [effect of a vortex on itself] of a vortex only enters when we deal with a 3-dimensional disturbance, and it is the self-induction that produces the difference between this and the original treatment [i.e. von Kármán's treatment] of the subject".

Rosenhead begins his study with a consideration of the behaviour of <u>small circular</u> vortices of radius ϵ that have m = 1 self-interactions resulting from 3-dimensional perturbations of wavelength $2\pi\ell^{-1}$ in the z-direction. Rosenhead defines a parameter

$$\eta = -\frac{1}{2}\, a^2\, \ell^2 \log(\ell\epsilon), \qquad (\ell\epsilon) < 1$$

which is claimed to be a measure of the self-induction. This parameter is introduced inconsistently into the von Kármán equations. The result remains a set of four first-order ordinary differential equations for the (x,y) velocities of the upper and lower streets. His paper goes on to discuss the dispersion relation which is now a function of η, and concludes (p.608) that there is "a distinct domain of instability in the neighbourhood of $\varphi = \pi/2$", where φ determines the initial perturbation.

We find Rosenhead's statement about the "self-induction" misleading, especially since η is a function of a and also applicable <u>only</u> when either $\ell \to 0$ or $\epsilon \to 0$. Rosenhead's claim (p.599) that for $\eta \to 0$ the stability investigations reduce to those of von Kármán is misdirected since our 2D calculations clearly show self- and mutual-

induction effects.

5. LAMINAR WAKE WITH A TRIANGULAR VELOCITY PROFILE

To simulate a laminar triangular velocity profile with a random perturbation, we distribute uniformly 1600 positive (light) and 1600 negative (dark) point vortex filaments over an area of 8 x 64 as shown in Figure 1.

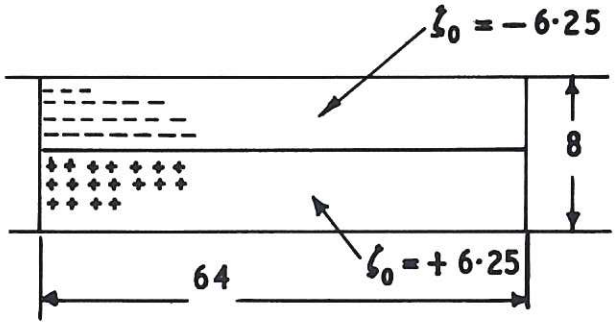

Figure 1. Initial distribution of vorticity in experiment I (x-periodic box).

This results in two strips of vorticity density $\zeta_0 = \pm 6.25$. The laminar state is perturbed by displacing each filament less than one lattice interval in a random and incompressible velocity field.

Figure 2 shows the longitudinal velocity profile obtained by

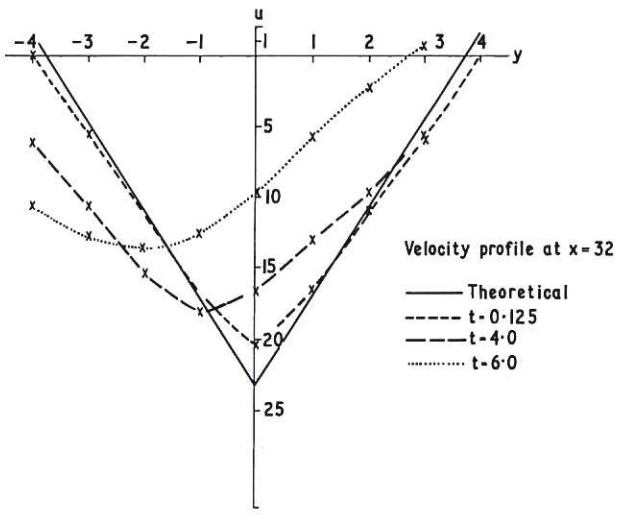

Figure 2. Initial velocity profiles for experiment I.

integrating the resultant ζ and choosing the constant of integration to result in zero x-momentum. The initial departure from the triangular profile is caused by the random perturbation as well as by the area-weighting method mentioned in Appendix 1.

The evolution of the perturbed triangular profile is shown in Figure 3. We will not discuss the linear phase of evolution as it has been well treated elsewhere (for example Zabusky and Deem,1971).

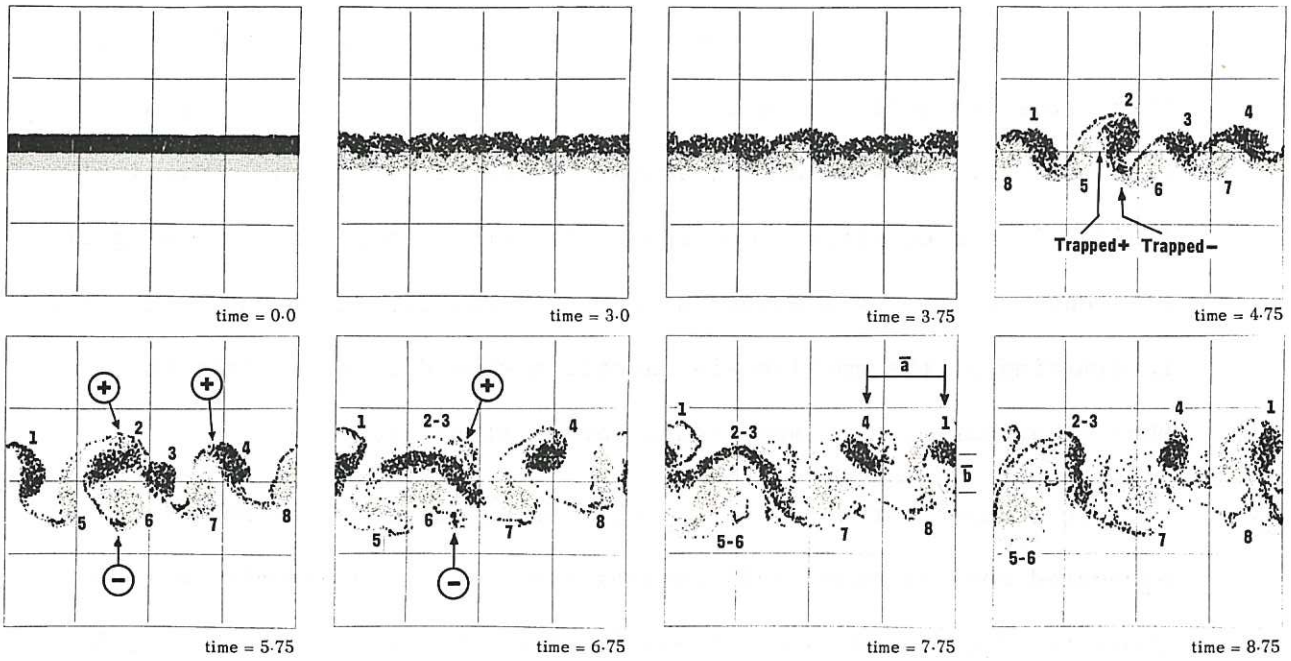

Fig. 3 Experiment I. Instability of a laminar wake subject to a small random perturbation. Fixed y-boundaries.

After approximately t = 4.2 the perturbation has grown and saturated because of non-linear effects. At t = 4.75 we see that 4 negative and 4 positive elongated vortex regions of varying area have formed into an asymmetric pattern. Note that at this stage small areas of positive or negative vorticity become "trapped" within or behind the larger vortex of opposite polarity. Between t = 5.0 and 6.75 two negative vortex regions (Nos.2 and 3) fuse into an elongated structure. At t = 6.75 we see positive vortex regions (Nos.5 and 6) begin to fuse. At t = 7.75 vortex region 1 is beginning to fuse with

region 2-3, but the process is inhibited by region5-6. Note that at t=7.75 the approximate transverse-to-longitudinal separation ratio is $\bar{b}/\bar{a} = 0.42$, that is, the wake width has increased by a factor of three due to the fusion, elongation, rotation and jetting of vortex "streams" or "arms", that is by convective processes. After t = 8.0 we have an irregular structure of 3 negative and 3 positive vortices per period with some mixing of positive and negative vortex filaments between the larger vortex regions. The situation corresponds roughly to an array of vortices staggered with respect to each other and moving in a weakly turbulent flow caused by "dispersion" of vortex filaments. This situation still prevails at t = 10.5 (not shown in Figure 3) with more filaments dispersed away from the main regions. Numerical finite-difference effects contribute to this dispersion and mixing of filaments and can be observed at t = 7.0. However for a short time the intermixing of the small-scale chaotic motion does not affect the mean behaviour of the large-scale vortex structures.

In figure 3 at t = 4.75 we see that negative vortex No.4 is elongated and its major axis rotates clockwise at a nonuniform rate whose average period is 4.7 (measured over the range $4.75 < t < 10.25$). A noninteracting ellipse (Kirchoff vortex, Lamb p.230) has a period $T_2 = \frac{4\pi}{\zeta_o}(\mu + 1)$ where $\mu = \frac{2 - \epsilon^2}{2\sqrt{1 - \epsilon^2}}$, ϵ being the eccentricity of the ellipse. A rough estimate of vortex No.4 gives $\epsilon^2 = 0.75$ so that $T_2 = 4.52$, close to that of the deformed strongly interacting elongated vortex region. Note that all vortex regions are drifting slowly to the left, whereas the distant irrotational fluid is streaming uniformly to the right.

In Figure 3 we observe that small trapped regions are converted around at the rotational frequency of the oppositely signed host vortex. This phenomenon was also observed and noted by Zabusky and

Deem (1971) and they designated these small regions as "secondary" vortices (see their Figure 8, p.368). Due to vortex rotation (in an appropriate frame) or "nutation" in the laboratory frame of reference, tracer particles, smoke or single vortex filaments will be transported to the opposite side of the vortex street, a phenomenon observed by Zdravkovich (1969, Section 3 and Figure 3). Thus, we have an enhanced transport of material across a flow due to convection by vortex states formed as a result of a linear instability of the system.

To summarize, in the early stages the linear instability driven by a particular random perturbation yields eight large vortices staggered with respect to each other. At t = 5.75 all vortices are elongated and nearly elliptical in shape but with different phases. The magnitude of the phases as well as the transverse separation between the vortices is a result of the initial conditions. This structure is unstable and like vortices are attracted and fuse in an attempt to find a more stable configuration. This transition from one vortex state to a more enduring state provides a heuristic explanation for the observations of Taneda (1959, Sec. 3 p. 847). At intermediate ($100 < R_e < 150$) and high ($R_e > 150$) Reynolds numbers the vortex streets in the wakes of cylinders (and flat plates) break down and reform such that the ratio of the effective wavelength of the secondary street to the primary street is two for intermediate-R and " ... of order 10". for high-R. The intermediate-R result could be explained as merely the fusion of nearest neighbour like signed vortex regions as observed above or as more clearly observed in Section 5 below. That is, viscous dissipation plays a small role in

comparison to the convective dynamical rearrangement of vortex filaments. Taneda observes this rearrangement or breakdown to occur again further downstream, a phenomenon consistent with our calculations. Taneda's high-R result is phenomenologically different for

".... after the primary Kármán vortex street breaks down the wake becomes turbulent, ... [a result already noted by Roshko in 1953]... . The turbulent wake continues to exist for a considerable distance. then there appears again a new Kármán vortex street". In the laboratory, the wake may develop small three-dimensional destabilizing fluctuations that enhance the fusion of larger vortex regions over a moderate distance. The enhancement process will cease when the three-dimensional fluctuations undergo viscous decay and we are left with a new two-dimensional quasi-equilibrium state.

6. STABLE CONFIGURATIONS

We now study the stability and dynamics of two pairs of Rankine vortices of radius R_o and density $\pm\zeta_o$. As shown in Figure 4, they are placed in a staggered fashion in a box with periodic boundary conditions in x, simulating states encountered in laboratory and computational experiments as described above.

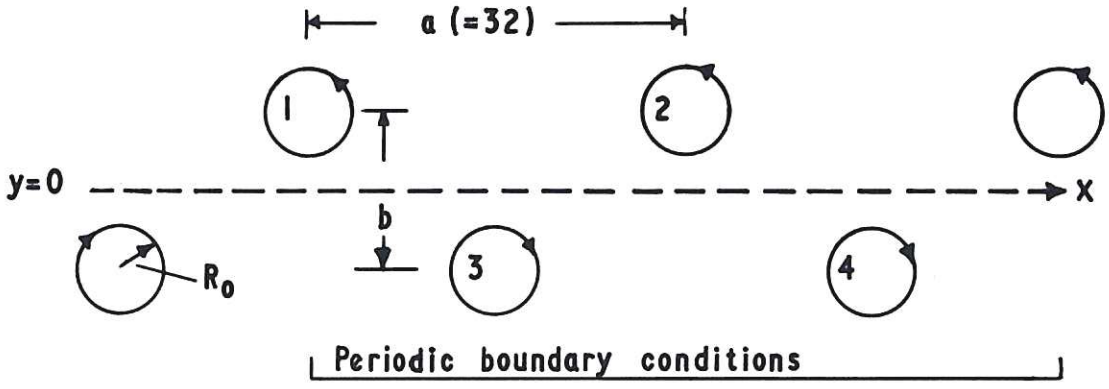

Figure 4. Arrangement of vortices.

Our realistic model considers finite sized vortices. If initially circular, their radius R_o is less than

$$R_M = \frac{a}{4}\sqrt{1 + 4\frac{b^2}{a^2}} = 9.17 \qquad \text{for } a = 32,\ \frac{b}{a} = 0.281,$$

if they are to be non-overlapping. The radius function of a vortex during subsequent dynamics can be written

$$r^2 = R_o^2 + \Sigma\ \alpha_m\, e^{im\theta}\ , \tag{23}$$

where r is measured from the initial center of the vortex

$$r_c = \frac{1}{2\pi}\int_o^{2\pi} \tilde{r}(\theta)\, d\theta\ .$$

For incompressible fluids there is no m = 0 mode and expression (23) conserves area ($= \frac{1}{2}\int_0^{2\pi} r^2(\theta)\, d\theta = \pi R_o^2$). It is natural to ask: how does the finite area of vortex regions affect the von Kármán stability conditions? The instability that leads to a rearrangement of the street results from a growth of the m = 1 mode for one or more vortices (see equation 23).

We have performed 4 different numerical experiments all using $\frac{b}{a} = 0.281$ in order to examine the stability properties of the arrangement sketched in Figure 4. Experiments II and III have initially 4 circular vortices of radius 3.0 and radius $\sqrt{35}$, respectively. In experiment II we introduce fixed y-boundaries, whilst III employs a doubly periodic geometry. The perturbation is in both cases a displacement of 1.0 in the y-direction of vortex 4, that is an m = 1 disturbance. Both experiments last for a time

interval of 9.0 corresponding to 576 discrete timesteps (see Table 1). In experiments IV and V we introduce very strong nonsymmetric perturbations: in experiment IV the major axes of positive vortices are inclined at 0.2 radian, whereas the major axes of negative vortices 3 and 4 are inclined at - 0.2 and 0 radian. Experiment V has vortex 1 with the major axis reduced from 7 to 4 so that the resulting density becomes $\frac{7}{4}$ times that of the other 3 vortices. In both experiments vortex 4 is given a <u>longitudinal</u> displacement (also an m = 1 disturbance) of - 6.0 . Experiments IV and V last only for a time interval of 3.0

From Figures 5 and 6 displaying the time evolution of experiments

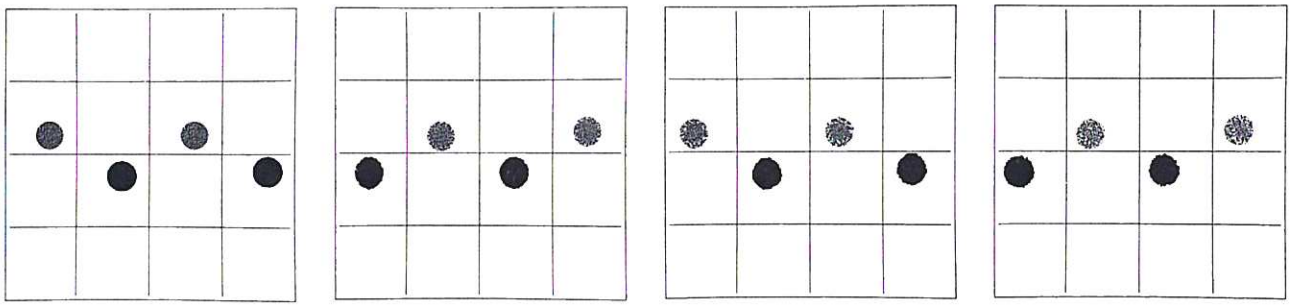

Fig. 5 Experiment II. Small vortices. b/a = 0.281. Fixed y-boundaries.

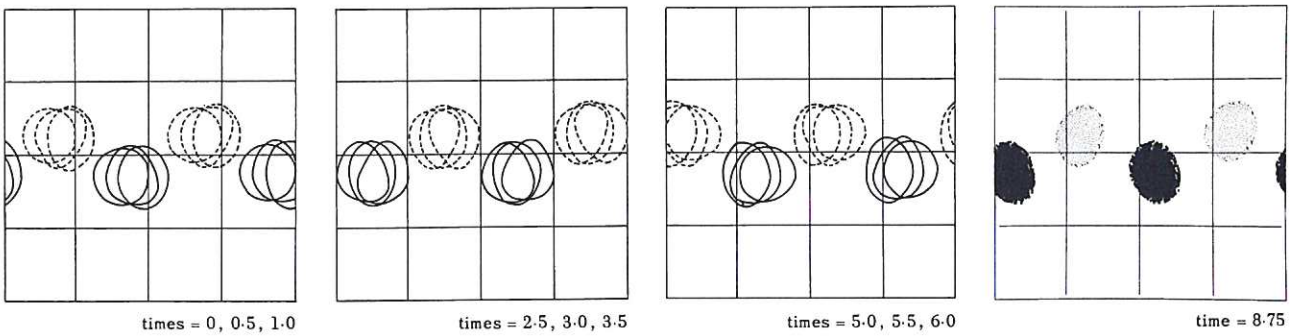

Fig. 6 Experiment III. Large vortices. b/a = 0.281. Periodic y-boundaries.
(The first three frames show only the vortex boundaries. The leftmost contour is the smallest time indicated)

CR 72 41
(rev. 6/72)

II and III it can be seen that both flow fields are apparently stable with respect to a small transverse perturbation. For all four vortices in both experiments the amplitude of the perturbation (say the position of the lowest point on the boundary) is found to be 1.0 (the same as the initial amplitude) and the period is 11.0 . This is in good agreement with the result given in (20), $T = 2\pi/\mathrm{Im}(\lambda) = 10.7$.

In both experiments the vortices rotate, deform and drift to the right with velocities nearly independent of their areas. Surface modes m = 2, 3 and higher develop from the mutual interactions of vortices. This is illustrated in Figure 6, where the first three frames each show only the boundaries of the vortex regions at three close times (left-most contour is the smallest time indicated). The amplitudes of the surface modes oscillate with time, such that after one period of rotation T_o the circular form is reached again. The period T_o is 1.9. For a non-interacting vortex in an infinite medium the period is 1.8 (Table 1). The difference is due to non-linear effects as well as coupling between modes of different m (see also section 8).

The fine scale structure and surface corrugations that develop (as exhibited at t = 8.75) are due to numerical area-weighting effects and do not disturb the large-scale dynamics.

Experiments IV and V (figures not shown) with different initial conditions and strong perturbations show similar effects, namely rotation, deformation and translation. In these short runs we observe an oscillation period of 8.0 (insteand of 11.0) and no sign of a growing perturbation. This may be a finite amplitude effect, however, the run duration is too small to make a definitive statement. The difference in periods could also be a measurement error since we

have less than 1/4 period of information.

The effect of the finite-difference algorithm on the small growth rates of a marginally stable system must be assessed. The variety of results presented here and the fact that parts of the vortex regions obviously extend into regions that are unstable for the point vortex system leads us to conclude that the observed stability is a property of the continuum, namely equation (2). The existence of negative energy modes resulting from area-conserving surface deformations contributes to this stability if the initial finite amplitude disturbance is not too large. We conclude that high-R finite area vortex streets have a small domain of stability around $b/a = 0.281$.

7. LARGE b/a ASYMMETRIC VORTEX STREET

We have performed 4 experiments with $b/a = 0.6$ as summarized in Table 2:

TABLE 2

Experiment	Figure	Area	Boundary Condition	Perturbation	Measured Growth Rate λ_m	Approx. Fusion Time
VI	7	large	fixed	large	0.62	5.5
VII	8	large	periodic	small	-	5.8
VIII	8	large	periodic	small	0.67	5.8
IX	9	small	periodic	small	0.67	6.9

In Figure 7 we display the time evolution of experiment VI, whilst Figure 8 shows both experiments VII and VIII. Experiment IX employing small vortices is shown in Figure 9.

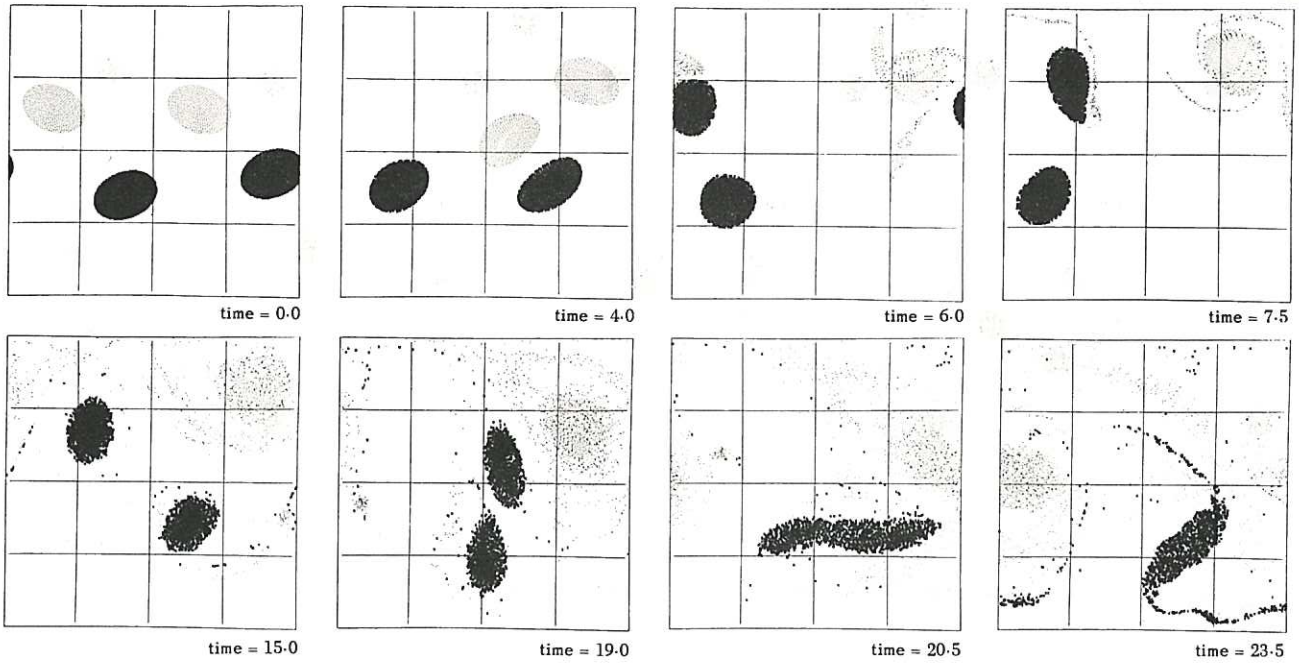

Fig. 7 Experiment VI. Large vortices. b/a = 0,6. Fixed y-boundaries.

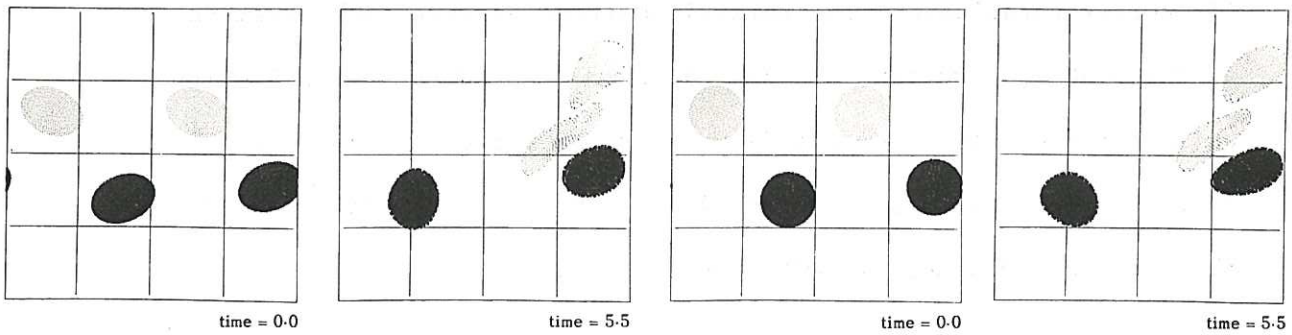

Experiment VII Experiment VIII

Fig. 8 Two initially different unstable configurations. b/a = 0.6. Periodic y-boundaries.

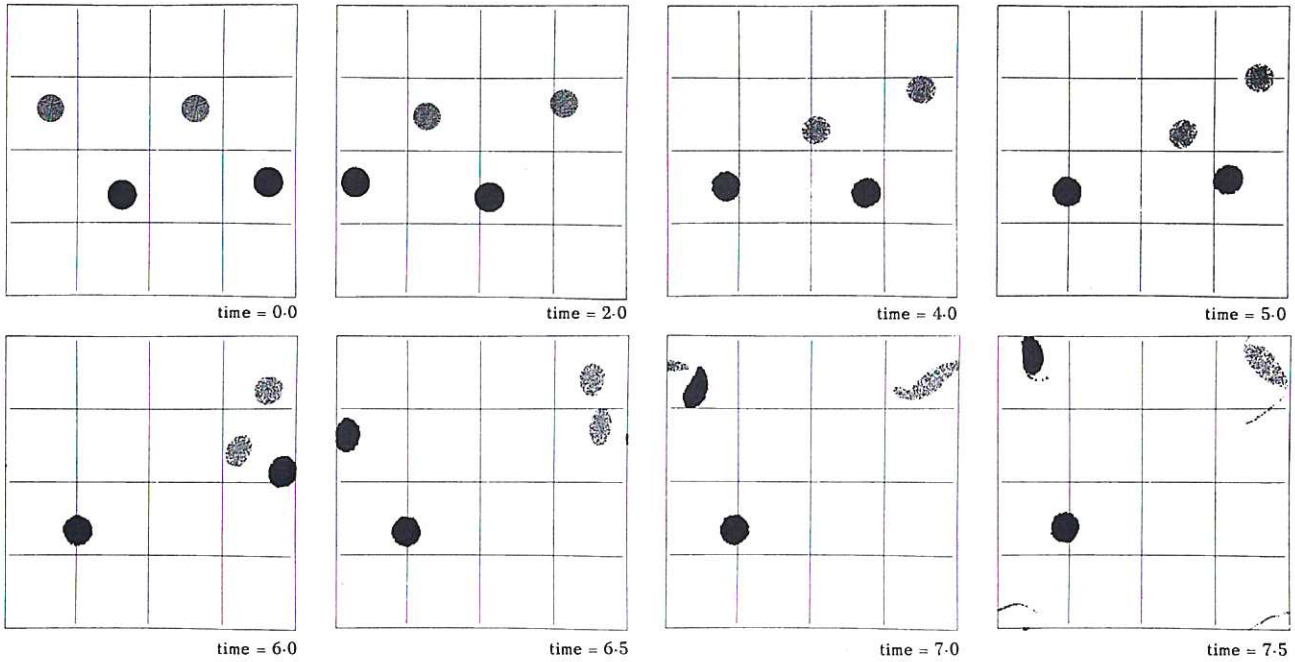

Fig. 9 Experiment IX. Small vortices. b/a = 0.6. Periodic y-boundaries.

Experiments VI, VII and VIII for the large-area vortices all show fusion of positive regions at about $t = 5.5$ (fixed boundary condition) and $t = 5.75$ (periodic boundary condition). Experiment IX for the small-area vortices shows fusion at about $t = 6.87$ (15 vortex rotations). The initial positive vertical perturbation of the center of vortex 4 is rapidly communicated to vortex 2 which while being ejected from the flow, attracts vortex 1. In experiment VI, although vortices 3 and 4 are close together at $t = 6.0$, the dynamics does not allow fusion until $t = 19.5$,

In Figure 10 we show the Δy_c of vortex 1 (moving downwards) for experiments VI, VIII and IX. Δy_c is the difference of the ordinates of the centre of the vortices

$$\Delta y_c = y_c(t) - y_c(o)$$

as measured from enlarged figures similar to those given in this paper and have an accuracy of $\pm$ 0.3 units. The motion of lower vortices 3 and 4 is initially oscillatory. The measured growth rate

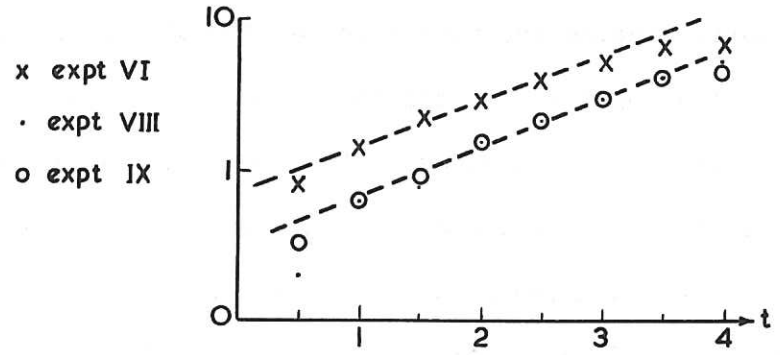

Figure 10. Growth of vortex center deviations, Δy_c, and measured growth rates for systems with (b/a) = 0.6 .

given in Table 2 shows a larger value for the larger area vortex and both are about 30% larger than the 0.481 for the point vortex system. This increase is undoubtedly due to the facts that: the vortex extends into "more unstable" regions, that is where the "effective" growth rate experienced by a point vortex is larger than that experienced by a point vortex at the centre of the finite area region; and finite-amplitude effects are important early in the dynamics. (Note that at t = 2, Δy_c = 2.5 units).

At later times when the dynamics are non-linear and there are large distortions to the vortex surface (m = 2, 3, ...), the rate of approach of like-signed large vortices is enhanced leading to a smaller fusion time. We find no significant change in the growth rate when the area is changed by a factor of $\frac{35}{9}$.

Beyond fusion, in the interval t = 7 - 19 (see Figure 7) the centroid of the fusion vortex is nearly stationary at the upper right and the two remaining vortices undergo precession. When they approach after t = 7.5, the vortex nearest to the fusion vortex is perturbed by the latter, i.e. a large m = 2 mode develops. At

t = 18,5 the two negative vortices have completed a full precession around their mutual centre and have also moved $\frac{1}{3}$ of the period in the + x-direction. The upper vortex and the fusion vortex now form a binary system which travels downward. The lower vortex cannot move further downward (fixed boundary condition), hence the two negative vortices fuse. The elongated shape of the resulting vortex at t = 20.5 is a result of the lower y-boundary being fixed, since a circular or slightly elliptic shape would give rise to a net motion towards the lower boundary. At t = 23.5 we note that the elongated vortex has contracted and thrown off spiral arms. The final result is then a "secondary" vortex street, with larger regions of positive and negative vorticity in asymmetric or staggered positions.

The dispersion and mixing of small-scale positive and negative vortex filaments between the larger vortex regions are strongly affected by numerical truncation errors, but play an insignificant role. This is analogous to real finite but high-R systems where small scales are dissipated. Two-dimensional fluid dynamic systems are known to seek states with larger scales (energy flowing to longer modes). This represents a new kind of condensation phenomenon.

8. COLLINEAR ASYMMETRIC VORTEX STREET - A STANDING WAVE

The collinear (b/a = 0) asymmetric vortex street (see Figure 11) is initially a standing wave with zero velocity

$$V_o = (\Gamma_o/2a) \tanh(\pi b/a) = 0 .$$

Koopman (1967, p.508) has shown that such a configuration can be generated in the laboratory by oscillating the cylinder transverse to the direction of flow. (In essence pockets of vorticity are detached from the cylinder at times that correspond to the transverse motion of the pocket across the axis of the flow). The results

obtained in our experiment X show linear instability regions followed by a strikingly new phenomenon -- the fission of one vortex.

A transverse perturbation is given to vortex 4 (the fourth on the line) and it grows during $0 < t < 6.0$, while the centre of vortex 3 is slightly displaced downwards. The measured initial growth rate is

$$\lambda_m = 0.41 \quad ,$$

smaller than the point-vortex value of 0.59.

Qualitatively, one may explain this reduction by noting that the outer areas of the collinear vortices are in spatial regions where the growth rate of a point vortex is smaller. That is, a first approximation to the growth rate of a finite-area system may be obtained by weighting the vorticity distribution with the growth rate due to that vorticity treated as a point-vortex system.

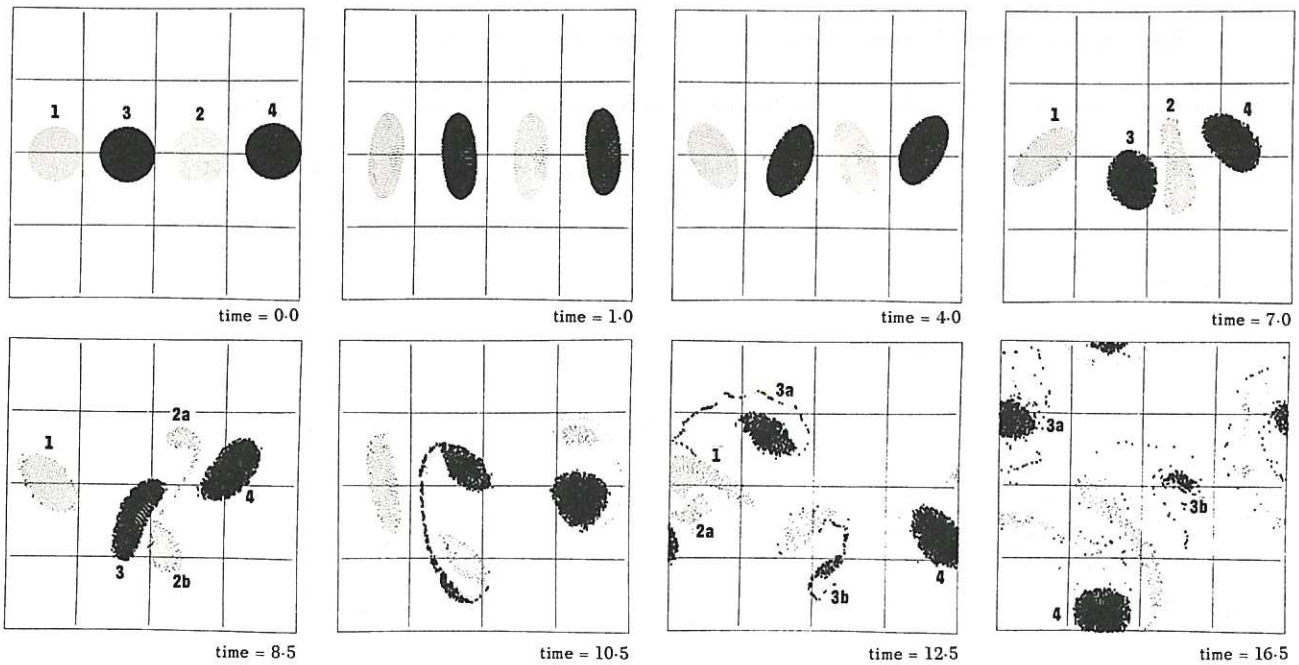

Fig. 11 Experiment X. Large vortices. b/a = 0.0. Periodic y-boundaries.

Strong m = 2 perturbations develop immediately because of the mutual interaction between vortices. Their period (measured during $0 < t < 4.0$) is about 4.0 - 4.5. The increase over the period of small amplitude m = 2 modes on a non-interacting vortex ($T_{m=2} = 3.6 \approx 2\ T_o$) arises because of the close interaction with nearby vortices, i.e. a non-linear effect. At $5.0 < t < 7.0$ we see that oscillations of the high m-modes (mainly m = 2) are no longer in phase because the applied disturbance has become large. At t = 7.0 there is an explosive growth of the m = 2 mode on vortex 2 causing it to undergo a fission process. The upper fission product is left nearly free while the lower fission product is trapped below vortex 3. At t = 12.5 the upper fission product fuses with vortex 1 and much later at t = 16.5 the lower fission product fuses with vortex 1. At this time we still have a fission product from vortex 3 in the centre of the frame.

The fission of large-area regions may be a common feature for collinear asymmetric streets and is the result of strong self-consistent vortex interactions. For smaller values of the interaction parameter $\eta = \frac{2R}{a}$ we will get only the predicted m = 1 instability, followed by fusion as in experiments VI to IX. The initial amplitude of the standing wave is a function of η, e.g. $\Psi_m \sim (\eta)^m\ e^{im\theta}$, where Ψ_m is the stream function associated with mode m (Christiansen, Taylor and Roberts 1972). This means that the standing wave represents a physical system whose stability properties strongly depend on the amplitude of the wave; indeed a truly non-linear situation.

An obvious question can be posed: How does the slightly perturbed system evolve if $0 < b/a < .281$? If the perturbation to both upper vortices is small then both upper vortex regions will rise at a rate which decreases in time as they approach a "stable band" around 0.281. The assumption of a decreasing rate is consistent with the observed lower growth rate of the collinear finite-area street described above and also with the Zabusky-Deem (1971) calculations as illustrated in their Figure 11b, where the transverse coordinate of the vortex is plotted versus time*. It also accounts for the experimental observation shown by Wille (1960) in his Figure 3. Here he presents a graph of the growth of a "corrected" ratio, $(b/a)_c$, versus distance behind a circular cylinder in water. The separation ratio begins at $(b/a)_c \simeq 0.1$ and slowly grows to an asymptote $(b/a)_c = 0.37$. The $(b/a)_c$ ratio then seems to oscillate around the asymptote (we see a slight decrease followed by an increase). According to Section 6 above, we conclude that the vortex regions are oscillating in a quasistable region. We are not sure if $(b/a)_c = 0.37$ is an estimate of the upper boundary of the "stable band" or whether there is a systematic error in reducing the data to $(b/a)_c$. Furthermore, if the perturbation is sufficiently non uniform and/or strong, the rising vortex regions may "pass through" the stable band and undergo fusion as described in Section 7.

9. DISCUSSION AND CONCLUSION

In this paper we have shown that the measured growth rates of finite-area vortex streets differ from those of corresponding point vortex systems (von Kármán systems). For small and moderate areas the difference is weakly dependent upon area and shape, but strongly dependent upon $(b/a)_c$ as illustrated in Figure 12. In this figure

---

* The b/a ratio obtained in their Runs 35 and 36 was erroneously stated as 0.24 (Equation 3.3). It should be 0.466, as one obtains by measurement in Figure 8 or from the simple ratio (4/8.38), where 4 is evident in Figure 11b.

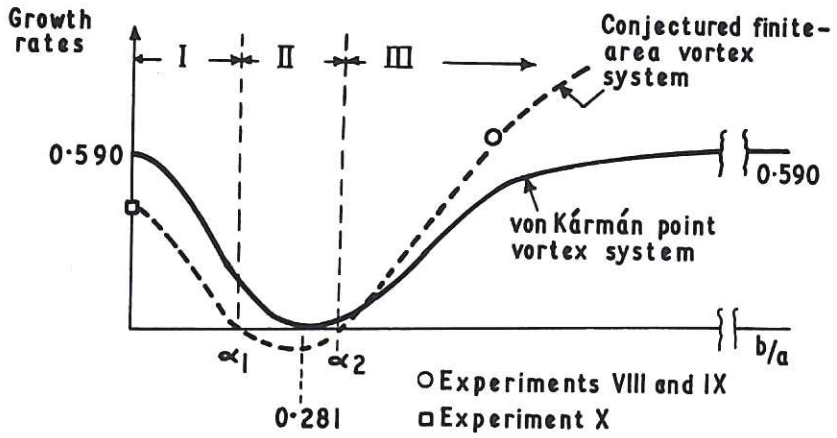

Figure 12. Perturbation theory growth rates: von Karman dispersion relation for asymmetric point vortex system compared with a corresponding moderate area system.

we conjecture that there exists a region (α_1 , α_2) on the (b/a) axis

$$\alpha_1 < 0.281 < \alpha_2 \quad ,$$

where the growth rate is negative, that is, the presence of negative-energy modes on the surface of finite-area vortex systems is stabilizing. Furthermore, because the vorticity is distributed the growth rate is reduced in regions I and II and increased in region III.

In the initial phases of evolution of an unstable laminar shear profile we have also observed an enhanced transport of vorticity across the dominant flow direction. This results from large-scale convection produced by vortex rotation (or "nutation"). As the vortex street is forming, small oppositely-signed ("secondary") vortices appear across the flow, as illustrated in Figure 3. Smoke or other contaminant particles will also undergo convective transport. These results are also consistent with experiment.

At long times, systems with $b/a > 0.281$ are unstable. Like-signed regions of vorticity attract and finally fuse (coalesce or "condense"). For a collinear asymmetric vortex street, we observed a linear growth phase followed by a rapid fission of one vortex, undoubtedly due to the high-shear field produced by the nearest-neighbour oppositely-signed vortex regions. This symmetry breakdown permits a rapid fusion of like-signed vortex regions at later time. These are strictly inviscid phenomena for they are in good agreement with those obtained previously by Zabusky, Deem et al, who solved the primitive Navier-Stokes equation with a high Reynolds number.

For comparison with laboratory experiments, these late time two-dimensional computational results should be considered qualitative and heuristic as three-dimensional motions are probably generated during the breakdown and rapid rearrangement stages. Vortex structures in the environment of a two-dimensional wind tunnel can have a longer lifetime than induced three-dimensional fluctuations. Thus our results qualitatively account for the vortex "breakdown" and subsequent wavelength increase of vortex streets observed in "two-dimensional" laboratory experiments by Taneda and others.

Acknowledgments

One of the authors, N J Zabusky, would like to acknowledge the support of the John Simon Guggenheim Memorial Foundation and Bell Laboratories, Inc. He also acknowledges the hospitality of Professor L C Woods and the Oxford University Mathematical Institute, and of Professor C L Pekeris and the Applied Mathematics Department of the Weizmann Institute, where parts of the manuscript were written. Both authors would like to thank Dr K V Roberts for his continued interest in this work, and David Howes for helpful assistance.

References

AMSDEN, A A, 1966. The particle-in-cell method for the calculation of the dynamics of compressible fluids. Los Alamos Scientific Report LA-3466.

BASSETT, A B, 1888. A treatise on hydrodynamics. Dover Publications Inc. (Corrected republication 1961).

BEAVERS, G S and WILSON, T A, 1970. Vortex growth in jets. J.Fluid Mech. 44, 97.

CHRISTIANSEN, J P and ROBERTS, K V, 1969. Rotational flows in a simple two-dimensional hydrodynamic fluid. Proceedings of the Computational Physics Conference at Culham Laboratory, July 1969. Vol. II, paper 40.

CHRISTIANSEN, J P, 1970. VORTEX - a two-dimensional hydrodynamics simulation code. UKAEA Culham Laboratory Report CLM-R106. Available from HMSO.

CHRISTIANSEN, J P, 1971. Numerical simulation of hydrodynamics by the method of point vortices. UKAEA Culham Report CLM-P282 submitted for publication in Journal of Computational Physics.

CHRISTIANSEN, J P and HOCKNEY, R W, 1971. DELSQPHI, a two-dimensional Poisson-solver program. Comp.Phys.Comm. 2, 127.

CHRISTIANSEN, J P, TAYLOR, J B and ROBERTS, K V, 1972. The interaction between finite-sized vortices in two-dimensional ideal fluids. To be submitted for publication.

DEEM, G S, HARDIN, R and ZABUSKY, N J, 1971. Computer-generated film on instability and turbulence of two-dimensional incompressible fluids. Bell Laboratories (unpublished).

HARLOW, F H, 1964. The particle-in-cell computing method for fluid dynamics. Methods in Computational Physics, 3, Fundamental Methods in Hydrodynamics. Editors B Alder, S Fernbach and M Rotenberg. Academic Press, New York. pp. 319-343.

KOCHIN, N E, KIEBEL, I A and ROZE, N V, 1964. Theoretical hydromechanics, Interscience Publishers,John Wiley & Sons,Inc. New York.

KOOPMAN, G H, 1967. The vortex wake of vibrating cylinders at low Reynolds numbers. J.Fluid Mech. 28, 501.

LAMB, H, 1932. Hydrodynamics. 6th edition. Cambridge University Press.

ROBERTS, K V and CHRISTIANSEN, J P, 1972. Topics in computational fluid mechanics. To be submitted for publication in Computer Physics Communications.

ROSENHEAD, L, 1930. The spread of vorticity in the wake behind a cylinder. Proc.Roy.Soc. A. 127, 590.

ROSENHEAD, L, 1929. The Kármán street of vortices in a channel of finite breadth. Phil.Trans.A, 208, 275.

SATO, H and KURIKI, K, 1961. The mechanism of transition in the wake of a thin flat plate placed parallel to a uniform flow. J.Fluid Mech. 11, 321.

TANEDA, S, 1959. Downstream development of wakes behind cylinders. J.Phys.Soc.Japan, 14, 843.

TANEDA, S, 1965. Experimental investigation of vortex streets. J.Phys.Soc.Japan, 20, 1714.

WILLE, R. 1960. Kármán Vortex Street. Advances in Applied Mechanics, VI, p.273. Eds. H L Dryden and Th. von Kármán, Academic Press, New York.

ZABUSKY, N J and DEEM, G S, 1971. Dynamical evolution of two-dimensional unstable shear flows. J.Fluid Mech. 47, 353.

ZDRAVKOVICH, M M, 1968. Smoke observations of the wake of a group of three cylinders at low Reynolds number, J.Fluid Mech. 32, 339.

ZDRAVKOVICH, M M, 1969. Smoke observations of the formation of a Kármán vortex street. J.Fluid Mech. 37, 491.

APPENDIX 1

Suppose we are given N sets of coordinates (x_i, y_i). From these coordinates the vorticity ζ is evaluated on the mesh using an area-weighting technique (Harlow 1964, Amsden 1966). The stream function ψ in equation (4) is solved for by the Hockney technique (Christiansen and Hockney 1971). The fluid velocity, equation (3), is evaluated at mesh points by centred difference operations. To move the point vortices in their own velocity field a leapfrog time integration method is used so that a point vortex at time $t - \Delta t$ can be moved according to

$$\underline{r}\ (t + \Delta t) = \underline{r}\ (t - \Delta t) + \underline{u}\ (\underline{r}(t))\ 2\ \Delta t \quad , \qquad (A.1)$$

which approximates $\frac{d\underline{r}}{dt} = \underline{u}$. It is necessary to employ two sets of coordinates, one at even times $t + 2n\Delta t$, one at odd times $t + (2n + 1)\Delta t$. To evaluate the velocity $\underline{u}$ at the even position $\underline{r}(t)$ in order to move from the odd position, $\underline{r}\ (t - \Delta t)$, the area-weighting technique is used again to interpolate from the velocity values known at the mesh points. In our experiments the VORTEX code computes a value of Δt that does not violate the Courant-Friedrichs-Lewy stability condition

$$\Delta t < \frac{\Delta x}{|u_{max}|} \quad , \qquad (A.2)$$

where $|u_{max}|$ is the largest <u>particle</u> velocity and Δx is the constant mesh spacing ($\Delta x = \Delta y = 1.0$).

During each numerical experiment we monitor the conservation of linear momentum, kinetic energy, as well as the mean square vorticity,

or "enstrophy" by calculating

$$P_x = \sum_{i,j} u_x(i,j) \ , \ P_y = \sum_{i,j} u_y(i,j)$$

$$E = \sum_{i,j} u_x^{\,2} + u_y^{\,2}$$

$$\langle \zeta^2 \rangle = \sum_{i,j} \zeta^2(i,j) \quad .$$

The incompressibility condition is identically satisfied for u_x, u_y at the mesh points at all times, such that a variation in P_x and P_y is due to computer rounding off errors which are of the order 10^{-5} corresponding to 18 bits in a computer word. The variations in energy and enstrophy are due to the discretizations in time and space and reflect some of the inaccuracies of the model.

In the table below we list the temporal variations in E and $\langle \zeta^2 \rangle$. As a reference to Figures 3, 5, 6, 7, 8, 9 and 11 we form the rations $\frac{\Delta E}{E_o}$ and $\frac{\Delta \langle \zeta^2 \rangle}{\langle \zeta^2 \rangle_o}$, where E_o, $\langle \zeta^2 \rangle_o$ are the values at time $t = 0$ and ΔE, $\Delta \langle \zeta^2 \rangle$ are the deviations from these values at the time t_o indicated in the last frame.

The leapfrog scheme (equation A.1) will exhibit odd-even temporal numerical instabilities when applied to certain types of flows. The two alternating levels at times $(2n + 1)\Delta t$ and $2n\ \Delta t$ will increasingly diverge from their average. To suppress this "false" effect a smoothing procedure is applied at a certain frequency during the motion (Christiansen 1970).

Exp No.	$\frac{\Delta E}{E_o}$	$\frac{\Delta\langle\zeta^2\rangle}{\langle\zeta^2\rangle_o}$	t_o
I	1.49×10^{-2}	2.62×10	8.75
II	1.47×10^{-2}	5.10×10^{-2}	8.75
III	1.49×10^{-3}	8.20×10^{-2}	8.75
IV	1.33×10^{-3}	3.80×10^{-3}	3.0
V	2.17×10^{-3}	6.37×10^{-3}	3.0
VI	6.20×10^{-3}	2.95×10^{-1}	23.5
VII	1.77×10^{-3}	1.63×10^{-2}	5.5
VIII	1.46×10^{-3}	1.26×10^{-2}	5.5
IX	6.11×10^{-4}	5.77×10^{-3}	7.5
X	8.93×10^{-3}	2.14×10^{-1}	16.5

TABLE A.1

Temporal variations in energy and enstrophy for experiments I - X